Article

Qualitative Assessment of Skin Deformation: A Pilot Study

Alice V. Maceo
Las Vegas Metropolitan Police Department

Abstract: Friction ridge skin deforms each time it contacts a surface. The primary factors determining the limits of skin deformation under applied stress to a fixed surface are the elastic nature of the friction ridge skin and the structure of the hand or foot area contacting the surface. This pilot study explored the flexibility of the distal phalanx of two index fingers of a single donor when compressive stress (deposition pressure) and tangential stresses (vertical sheering stress, horizontal sheering stress, and torque) were applied to a smooth, flat surface. The flexibility of the skin was found to be dependent upon the amount of compressive stress applied, the direction of tangential stress, and ridge flows in the fingerprint pattern. In addition to exploring the limits of skin flexibility, the effects of these different stresses were studied in latent prints generated under these conditions. The latent prints displayed robust clues that permit interpretation of the skin deformation by properly trained specialists.

Introduction

The pliable nature of the friction ridge skin permits deformation (change in the shape or form that is due to an applied stress) when the skin contacts a fixed surface. Skin undergoes a distinctive type of deformation, called "elastic deformation" [1-5]. Elastic deformation occurs when a material returns to its original shape after the stress is removed [6, 7].

Received December 8, 2008; accepted February 3, 2009

Through repeated examination of friction ridge impressions deposited under various stresses, the practitioner develops an intuitive understanding of the flexibility of the skin and the limits of skin deformation. The practitioner, however, may lack a vocabulary to describe these phenomena or may not understand the significance of visual clues in the friction ridge impressions. Additionally, because there is little published on aspects of skin deformation as it applies to latent print examination, the practitioner may not be accurately assessing the effects of skin deformation. A review of the common literature in the latent print community (textbooks and the *Journal of Forensic Identification*) revealed only two substantive discussions of skin deformation as it pertains to latent print analysis. James Cowger introduces the topic in *Friction Ridge Skin: Comparison and Identification of Fingerprints* [8], and David Ashbaugh delves deeper into the topic in *Quantitative-Qualitative Friction Ridge Analysis: An Introduction to Basic and Advanced Ridgeology* [9]. Although both Cowger and Ashbaugh offer good general discussions and examples of distortion, both lack details of a systematic study. Unless the practitioner has made a personal study of skin deformation, the assessment of deformation is, at best, information learned from a reliable source, and, at worst, a guess.

There is a vast amount of literature in the fields of biometrics and robotics describing the quantitative (measurable) aspects of skin deformation [2-5, 10-12]. In the biometric world, skin deformation is studied to create or enhance matching algorithms for automated fingerprint recognition systems (e.g., AFIS). The robotics industry studies the mechanics of skin to design robotic hands that can manipulate objects, particularly for manufacturing processes. In addition to biometric and robotic applications, computational methods that account for the flexibility of the skin have been developed to assess the similarity of fingerprints for possible application in casework [13]. It was not the intention of this study to attempt to quantify or measure skin deformation. The goals of this pilot study were to (1) discuss the anatomy of the hand and skin as it contributes to the flexibility of the skin, (2) illustrate the effects of skin deformation of the distal phalanx under controlled circumstances, and (3) provide a common language to describe the visible effects of basic skin deformation in latent fingerprints.

Anatomy of the Hand

The index, middle, ring, and little fingers of the hand each have three phalanges: distal, medial, and proximal. The distal interphalangeal joint crease separates the distal and medial phalanges. The proximal interphalangeal joint crease separates the medial and proximal phalanges. The proximal phalanges of the fingers and the palm are separated by the palmar digital crease. The thumb does not have a medial phalanx or a proximal interphalangeal joint crease. The palm is separated into four key regions: thenar, hypothenar, metacarpal (interdigital), and midpalmar space. The palm typically has three major creases: distal palmar crease, proximal palmar crease, and longitudinal thenar crease. Figure 1 illustrates the outer anatomy of the palmar side of the hand.

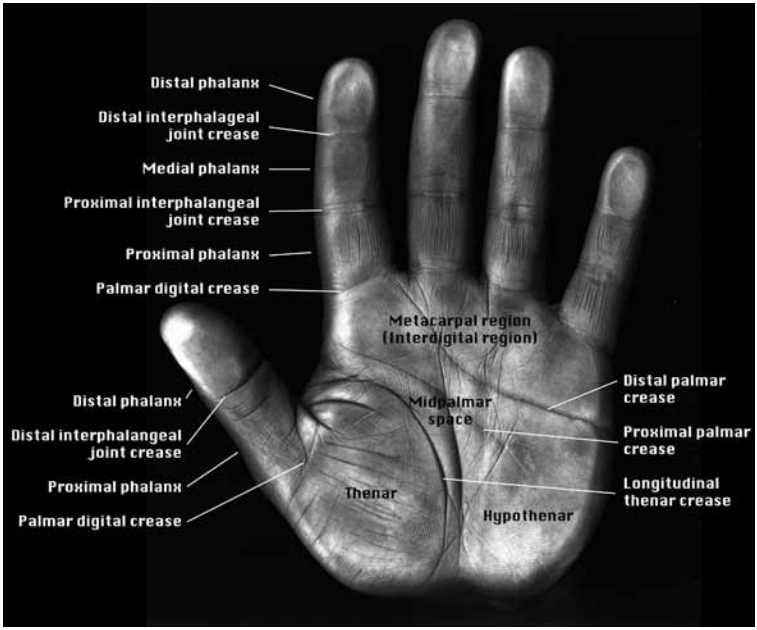

Figure 1

Regions of the palmar side of the hand.

The palmar side of the hand is covered with thick, glabrous skin – the friction ridge skin. The skin is composed of three primary layers: the hypodermis, dermis, and epidermis (Figure 2). The hypodermis contains subcutaneous fat embedded in a fibrous network. The fibrous network molds the fat into chambers of various sizes and provides protection to the underlying tissues (e.g., muscles and ligaments) [14]. The dermis provides the skin elasticity with its own network of fibers and gelatinous ground substance. The epidermis is the outermost protective barrier. All three layers of the skin contain sensory organs that transmit the sensation of touch.

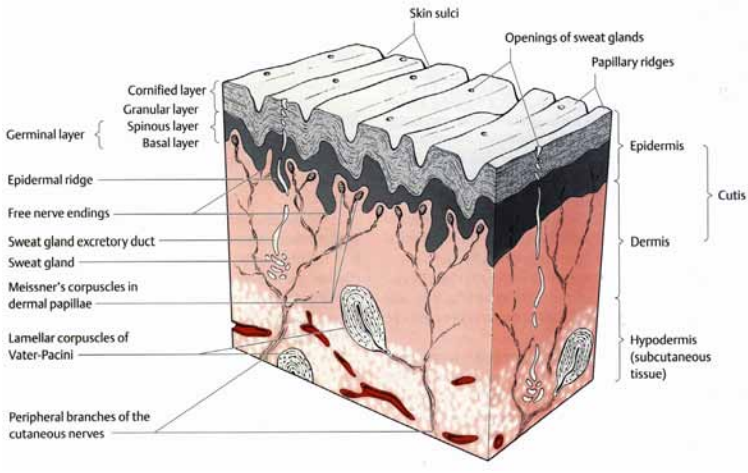

Figure 2

Structure of friction ridge skin [14].
(Reprinted with permission from Thieme.)

Beneath the thick layer of skin, the palmar side of the hand has a vast network of connective tissue fibers (palmar aponeurosis). These fibers support the structural elements of the hand (bones, tendons, and ligaments) and anchor the skin to the hand. The fibers of the palmar aponeurosis radiate from the palmaris longus tendon at the wrist toward the bases of the fingers. As shown in Figure 3, the palmar aponeurosis is a web of transverse, longitudinal, and perpendicular bands of fibers. These fibers connect to the major ligaments of the hand. The palmar aponeurosis also supports the recessed areas of the hand and resists forces that flatten the hand [14]. (Latent print examiners are familiar with the difficulty of recording the skin of the midpalmar region because of the inability to flatten the hand.) The palmar aponeurosis provides general attachment for the palmar skin; however, it is more firmly attached to the skin at the major palm creases [14] and the interphalangeal joint creases [14]. The tight attachment of the aponeurosis to the skin prevents the skin from slipping against the deeper tissues of the hand (e.g., muscle or ligaments) [14] and creates distinctive physical borders within the palm and fingers. The distinctive physical borders may create distinctive borders when considering skin deformation. In other words, deformation may not be exhibited globally across the palm; it may have regional impact because of the borders established by the major creases. This topic requires additional research and it cannot be assumed that deformation in the palm or lower phalanges (medial and proximal) will be the same as the deformation of the distal phalanx as presented in this study.

Beneath the palmar aponeurosis, the musculature of the palm is revealed. Figure 4 illustrates the superficial musculature of the thenar and hypothenar. The thenar is predominantly formed by the muscles of the thumb and is the most mobile portion of the palm [14]. Twenty-five percent of the muscles in the hand are dedicated to moving the thumb [14]. There is very little subcutaneous fat in the thenar region.

The hypothenar has three layers of muscle (Figure 4) buried under a thick layer of subcutaneous fat [14]. Schmidt and Lanz proposed that this thick layer of subcutaneous fat in the hypothenar aids in grasping objects: “It is possible that the skin molds itself to the surface of the object while protecting deeper soft tissue against pressure.” [14]

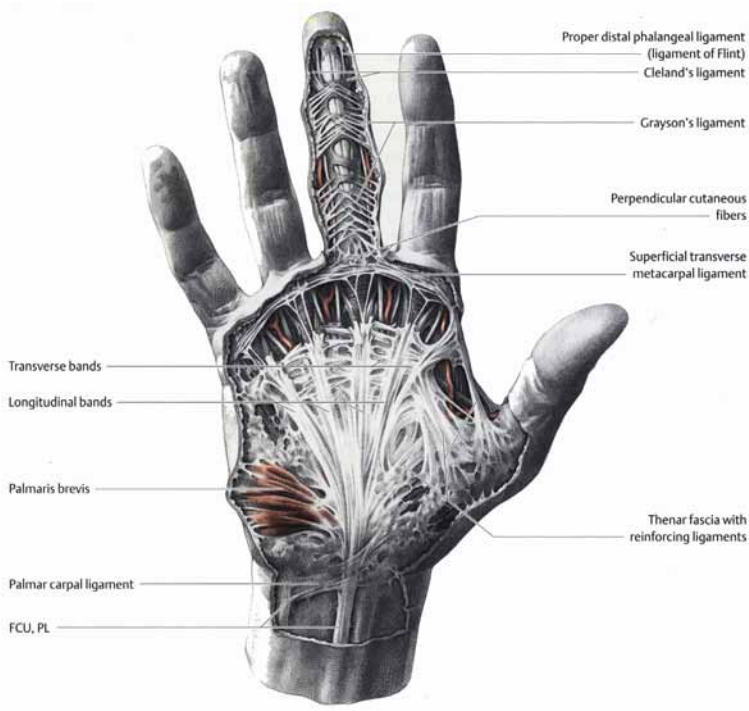

Figure 3

Palmar aponeurosis - subcutaneous fibers connecting the skin to the underlying structures of the hand. FCU = Flexor carpi ulnaris tendon. PL = Palmaris longus tendon [14]. (Reprinted with permission from Thieme.)

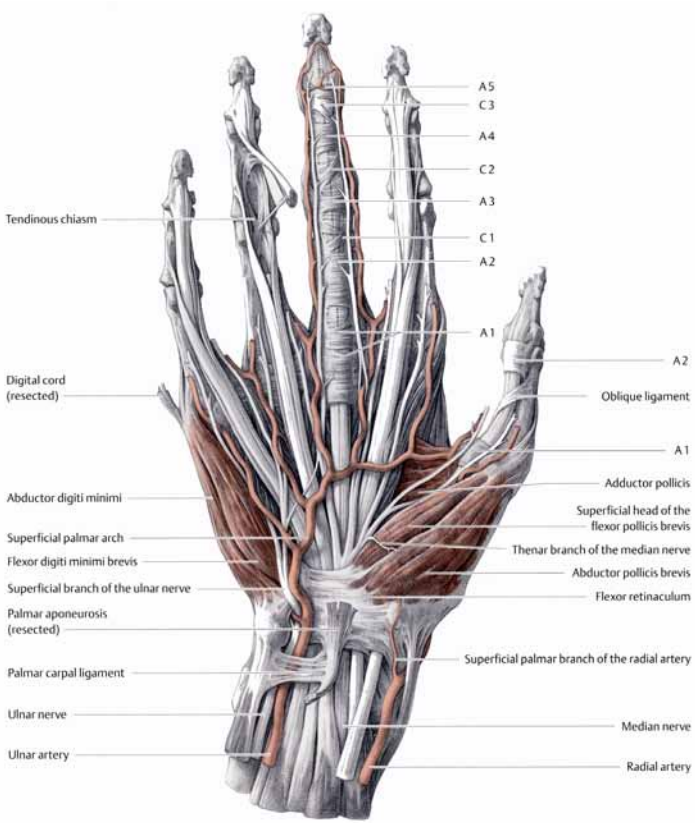

Figure 4

Superficial structures of the palm. The musculature of the thenar and hypothenar are colored red [14]. (Reprinted with permission from Thieme.)

The midpalmar space, largely covered by the palmar aponeurosis (Figure 3), houses the flexor tendons of the fingers, the lumbricals (small muscles attached to the fingers), and the nerve fibers that extend into the fingers [14]. The structures of the midpalmar region are embedded in a protective layer of fat in the center of the palm [14].

The metacarpal (interdigital) region of the palm stabilizes the highly mobile fingers with the metacarpal transverse ligament (Figure 3). The transverse metacarpal ligament spans the width (radial to ulnar side) of the palm and is connected to the metacarpophalangeal joints of the finger (where the fingers connect to the palm) [14]. The metacarpal region also contains a protective layer of subcutaneous fat. Schmidt and Lanz highlight the importance of the transverse metacarpal ligament: "With its firm connections with the metacarpals and the palmar aponeurosis and skin, it helps to contain the soft tissue when the hand grips objects." [14]

The innermost reaches of the hand contain the bone structure and the fine lumbrical muscles and tendons (Figure 5). The lumbrical muscles aid in extension of the fingers (flexion of the fingers is produced by flexor muscles in the palm) [14]. Figure 5 also displays the bone structure of the hand: the ulna and radius of the forearm, the carpals of the wrist, the metacarpals of the palm, and the phalanges of the fingers. Note the distal phalanges end in a distinctive "tuft" of bone.

An x-ray image of the distal phalanx of a finger in Figure 6 reveals the paddlelike tuft of the distal phalange (A). Note the position of the paddlelike tuft of the bone just above the core (B) of the fingerprint and the cushion of fat and dermis between the end of the bone and the extreme tip of the finger (C). The significance of A, B, and C in Figure 6 will be discussed in the Mechanics of Touch section.

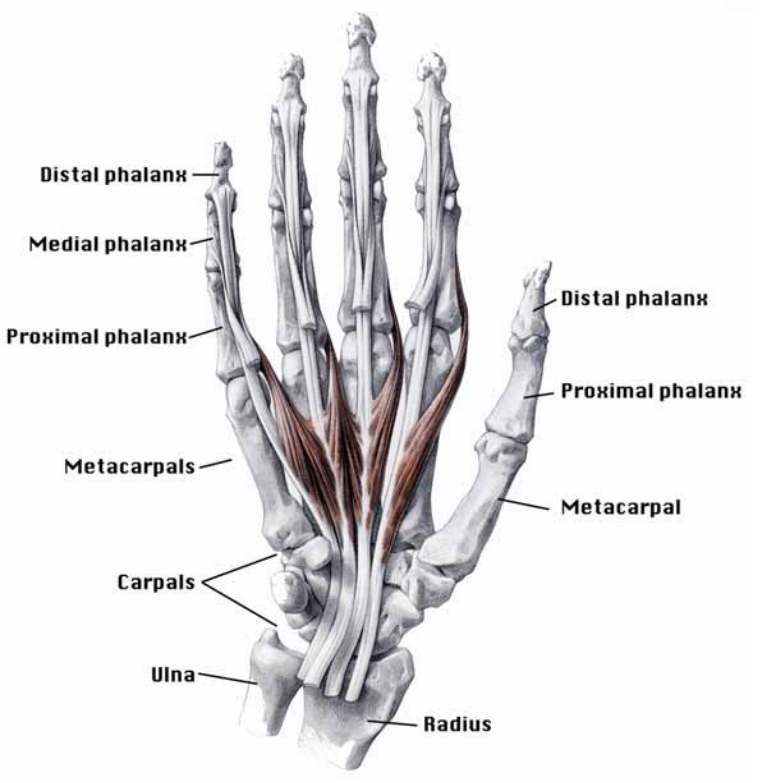

Figure 5

Lumbrical muscles (in red) and bones of the hand [14]. (Adapted and reprinted with permission from Thieme.) Note the paddlelike tuft at the tip of the distal phalanges.

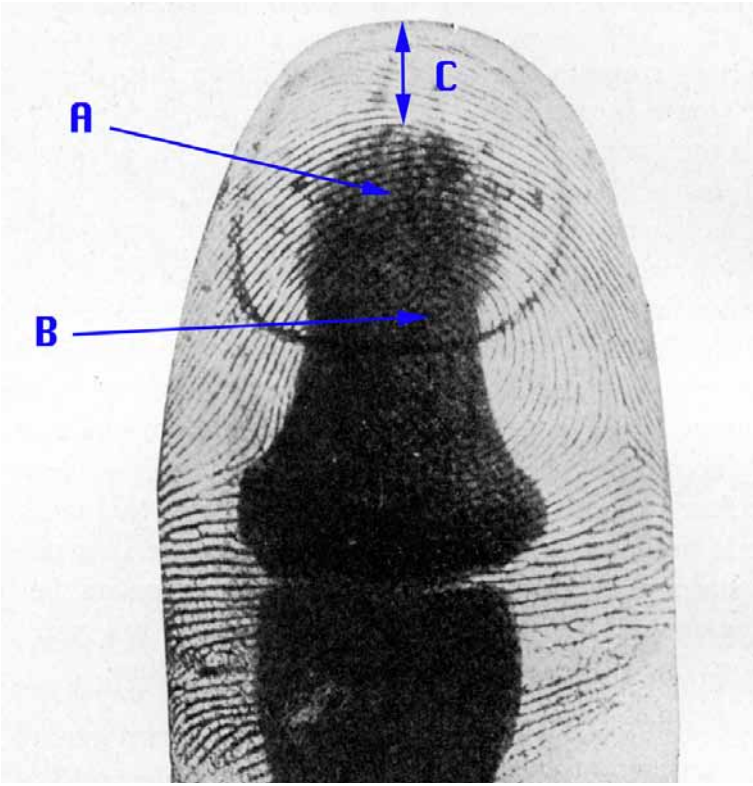

Figure 6

X-ray of the distal phalange [15]. (Adapted from Cummins & Midlo.) Arrows point to the paddlelike tuft of the distal phalange (A), the core of the fingerprint (B), and the cushioned tip of the finger (C).

The friction ridge skin, with its thick subcutaneous fat, is designed to withstand compressive stress. The fatty tissue in the pulp of the finger pad is structured into small chambers by fibrous connective tissue. These chambers prevent the fat from being pushed into other regions of the finger and form "cushions of varying size that mold to [the] shape of the object and improve the hand's grip" [14]. Figure 7 is a longitudinal cross-section of the distal phalanx. The retinacula of the skin in Figure 7 are the fibers that form the chambers of fatty tissue in the pulp of the finger. The pulp of the finger has distinctive borders. It is bordered distally by the free end of the fingernail, it is bordered laterally by the junction with the nonfriction ridge skin, and it is bordered proximally by the distal interphalangeal joint. According to Schmidt and Lanz: "The average length of the pulp is 27 mm in the index and middle fingers, 26 mm in the ring finger, and 22 mm in the little finger." [14]

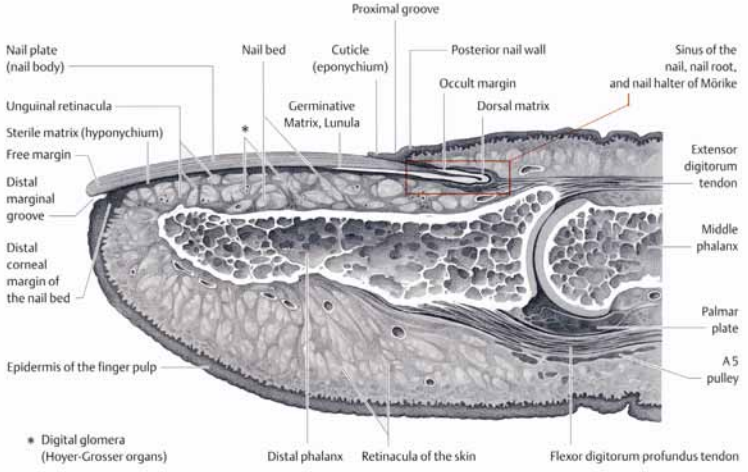

Figure 7

Longitudinal section through the distal phalanx [14]. (Reprinted with permission from Thieme.)

The fatty pulp of the finger is not uniform across the surface of the finger pad. It is divided into two regions: proximal pulp and distal pulp. The proximal pulp is defined as the pulp between the distal interphalangeal joint crease and the base of the tuft of the distal phalanx. The distal pulp is defined as the pulp from the tuft of the distal phalanx to the tip of the finger [14]. A network of fibers divides these two regions of pulp. The proximal pulp is thicker and more mobile than the distal pulp [14]. The distal pulp is divided into small, compact compartments of fat that are delineated by strong fibrous plates (Figure 7). This reinforced region of the distal pulp is designed to absorb significant amounts of pressure when objects are gripped or forcibly touched [14]. When considering skin deformation, the proximal portion of the finger pad is more flexible than the distal portion. Figure 8 demonstrates the outer regions of the finger that would correspond to the distal rigid finger pulp and the flexible proximal finger pulp.

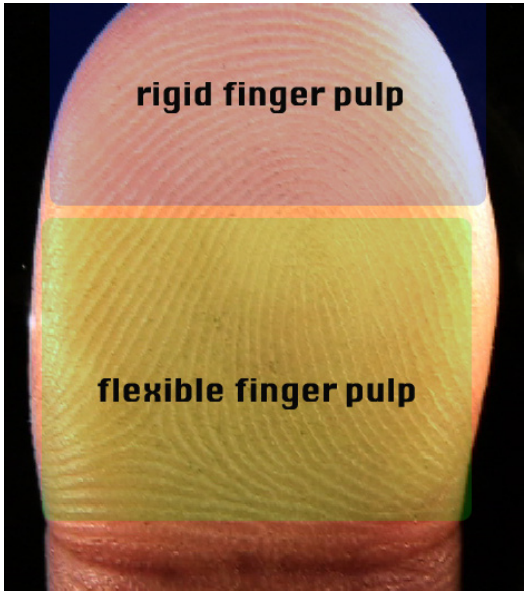

Figure 8

Outer region of the finger that corresponds to the underlying rigid distal finger pulp and flexible proximal finger pulp.

Specialized Adaptations of the Epidermis of the Friction Ridge Skin

As previously mentioned, the skin is composed of three primary layers: epidermis, dermis, and hypodermis. The outer epidermis is a protective layer of stacked cells; the predominant cells in the epidermis are keratinocytes. The dermis contains fibers and gelatinous ground substance and provides the skin flexibility. The hypodermis contains fat tissue that gives the body contours, protects underlying tissue (e.g., muscle and bone), and cushions the skin.

As shown in Figure 9, the epidermis has layers of keratinocytes in various stages of differentiation as they move toward the outer surface of the skin (stratum corneum). The stratum basale (basal layer) of the primary and secondary ridges produces the cells that maintain the surface ridges and furrows, respectively.

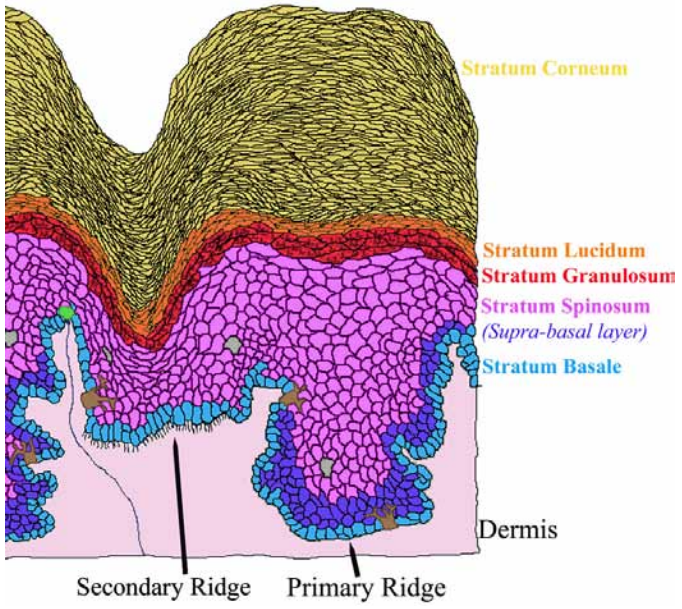

Figure 9

Layers of the epidermis.

The basal layer of the primary and secondary ridges contains keratinocytes. However, Lavker and Sun [16] demonstrated that the keratinocytes in the basal layer of the primary ridges (corresponding to the surface ridges) are different from the keratinocytes in the basal layer of the secondary ridges (corresponding to the surface furrows). With respect to skin deformation, the important distinction is the manner in which the basal cells are anchored to the dermis. The basal cells of the primary ridges have a relatively smooth attachment to the dermis. The basal cells of the secondary ridges have long "cytoplasmic projections" [16] that protrude into the dermis. These fingerlike structures afford the furrows greater anchorage to the dermis.

In addition to the structural differences between the basal keratinocytes in the primary and secondary ridges, Swensson et al. reported that different types of keratin are manufactured in these regions [17]. Keratin is the signature protein of the skin cells and provides an effective protective barrier to the environment. The keratin produced in the primary ridges (and corresponding surface ridges) is very rigid, whereas the keratin produced in the secondary ridges (and corresponding surface furrows) is quite flexible. Swensson describes the furrows as an elastic hinge between the ridges [17]. It is expected that stress on the ridges will transmit to the more flexible furrows. Given that the furrows must deform to accommodate the stress, the furrows require greater anchorage to the dermis via the fingerlike projections described by Lavker and Sun [16].

Mechanics of Touch

When the pad of a finger contacts an inflexible surface, like glass, the pad of the finger acts like an elastic sphere [2, 5]. When the finger is viewed in cross-section (Figure 10), the dynamic of the elastic sphere created by the pulp of the finger pad is evident. Once again, note the chambers of fat delineated by the retinacula of the skin.

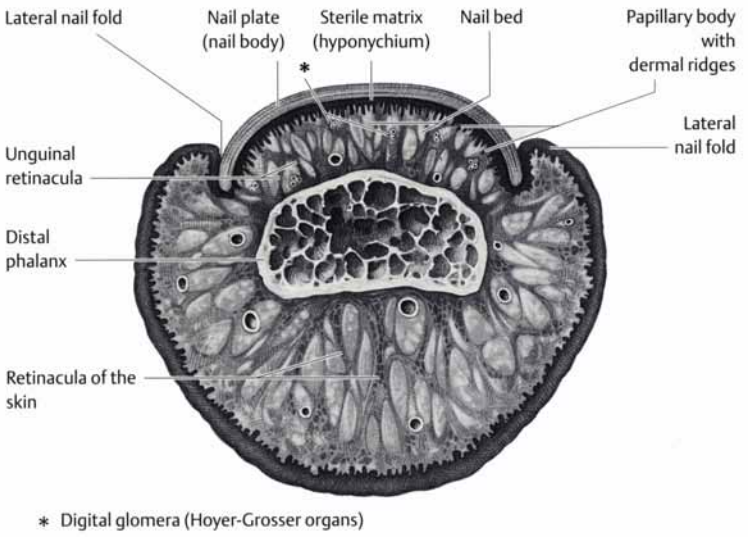

Figure 10

Cross-section of the finger through the distal phalanx [14]. (Reprinted with permission from Thieme.)

The greater the compressive force applied to the surface (deposition pressure), the greater the surface area of contact between the finger and the glass. Serina et al. demonstrated that the maximum contact surface area between a finger and a flat surface occurs at approximately 5.26 newtons of force [12]. The greatest increase in contact surface area between the finger and a flat surface took place from 0 to 1 newton; 69% of the contact region was obtained before the deposition force reached 1 newton [12]. In other words, from 0 to 1 newton, the pad of the finger was quite flexible and flattened onto the surface easily. Greater than 1 newton, there was little increase in the contact surface area and the finger acted as a stiff pad [12].

When the finger squarely contacts a surface (i.e., the finger is parallel to the surface), deposition pressure is greatest just above the core of the fingerprint pattern. This region is directly under the distal tuft of the bone. The deposition pressure gradually decreases toward the boundary of the finger [2, 18]. The high-pressure zone created by the bone causes the corresponding area of skin to "stick" onto the surface. The region of skin

surrounding this “stick” area is under less pressure and will deform (or “slip”) when sheering stress (pushing the finger one direction) or torque (twisting the finger) is applied [1, 5, 10]. The periphery of the finger is under very little pressure and generally moves freely as the finger moves. Figure 11 illustrates the region of “stick” centered just above the core, the surrounding region of “slip”, and the peripheral “free motion” region under low, medium, and high pressure. Note that the zone of slip (deformation) increases as the pressure increases.

When tangential force (sheering stress or torque) is applied to the finger, a partial slip occurs in the “slip” region prior to the finger completely sliding on the surface. This partial slip is called “incipient slip” [2, 5]. Under increasing tangential force, a “gross slip” will occur and the entire contact area of the finger slides on the surface. Fortunately for the practitioner studying exemplar prints and latent prints, the skin reacts to tangential forces in predictable ways.

Figure 11

Zones of deformation under low, medium, and high pressure.

As discussed earlier, the furrows act as flexible hinges between the ridges. As a result, the more parallel ridges in sequence, the greater the potential flexibility of that particular region. Figure 12 illustrates areas of numerous parallel ridges in two fingerprints. It will be demonstrated later how these regions respond to stress; however, the parallel ridges can be thought of as an accordion – expanding and compressing, depending on the force exerted across the finger. Given the pattern type of these two fingerprints (whorl and loop, respectively), the parallel ridges generally radiate like spokes from the core of the pattern area.

In addition to the high and low pressure areas caused by the bone and the significance of parallel ridges, another important anatomical feature of the finger that contributes to deformation is the composition of the finger pulp. As shown in Figure 7, there is finger pulp in the pad of the finger and at the tip of the finger. The pulp at the tip of the finger provides cushion for the distal phalanx when distal sheering stress is applied to the finger. Additionally, the skin on the proximal portion of the finger is more flexible because of the more flexible underlying pulp. This will have a significant impact when considering vertical sheering stress.

Figure 12

Zones of parallel ridge delineated by the blue arrows.

Materials and Methods

A digital video camera (Canon Optura 500) was secured under a piece of smooth glass and tethered directly to a laptop computer for direct capture of the videos. Video recordings were made of the two index fingers from one donor touching the glass. These two fingers were selected based on pattern type: one index finger was a symmetrical whorl and the other index finger was an asymmetrical loop (Figure 12). The fingers were charged with sebaceous natural secretions by wiping the fingers onto the forearm of the donor. The donor would recharge the residue after three or four touches.

The fingers were placed at a low angle to the glass (approximately 25°) and displaced vertically (distally and proximally) or horizontally (left or right) under low, medium, and high deposition pressure. Distances were tracked by placing a mark on the distal interphalangeal joint crease (a free motion area) and tracking the distance the mark traveled as a sheering stress was applied. The deposition pressure was not measured; it was determined by the donor and monitored by the author during filming to ensure relative consistency.

In addition to these sheering stresses, torque was also applied to each finger under low, medium, and high deposition pressure. The degree of rotation was measured by affixing a pointer to the nail of the finger and rotating the finger to the appropriate position on a marked grid. The whorl and loop were filmed rotating both clockwise and counter-clockwise.

Each video was later analyzed to determine the following:

- How did the stick and slip areas of the skin respond to stresses?
- What impact did the stress have on minutia placement?
- Was the skin more flexible under certain stresses?
- Did pattern type influence the deformation of the skin?

Although this study approached distortion from a qualitative perspective, there is some value in looking at measurements to evaluate whether the measurements concur with the visual data. For example, under high pressure, the loop pattern appeared to

be more flexible in one direction of torque versus the opposite; do the measurements confirm what appears in the video? Still images were taken from the video at the initial contact position of the finger and at the position of the finger just before the entire finger slid on the surface (gross slip). The distance the finger rotated or moved (vertically or laterally) was then measured via the Adobe Photoshop Ruler Tool. Only one to three measurements were available for each type of deformation and it is recognized that more data under controlled deposition pressure is needed to provide additional meaning to the data. Raw data is presented with limited interpretation.

After each video was recorded, the latent print deposited on the glass was developed with black powder, recovered with lifting tape, and preserved on a lift card. The latent prints were later analyzed to determine the following:

- How did movement of the finger and deformation of the skin translate into latent prints?
- What indicators of movement and deformation consistently reproduced?
- Were the effects of skin deformation dependent upon pattern type?

It should be noted that the latent print images were mirrored (laterally reversed) in order to compare the latent prints to the video.

Results

Compressive Stress

The first type of deformation explored was the most basic: compressive stress. Compressive stress is also referred to as "deposition pressure". As deposition pressure increased, more of the ellipsoid-shaped finger contacted the surface, and the width and length of the latent print increased. Figure 13 contains still video images of the skin and the resultant latent prints under low, medium, and high deposition pressure (A, B, and C, respectively). The arrows on the still video images point to the left edge of the finger, where it contacted the glass. Note the general elliptical shape of the resulting latent prints and the increase in size of the latent prints.

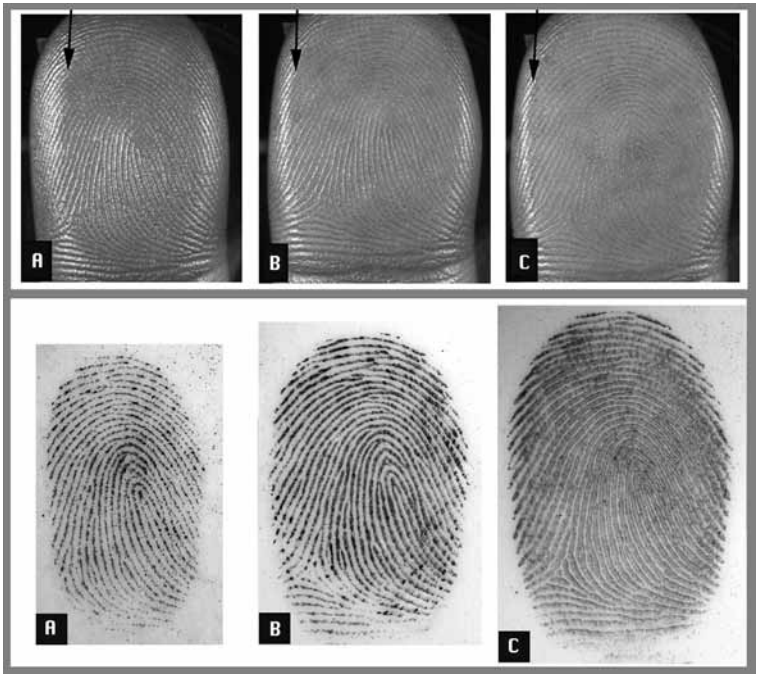

Figure 13

Finger contact area and resultant latent prints under low (A), medium (B), and high (C) deposition pressure.

In addition to the contact area of the finger increasing as the deposition pressure increased, the ridges and furrows were also affected. The ridges became wider and the furrows became narrower. Figure 14 contains still video images and latent prints under low, medium, and high pressure (A, B, and C, respectively). The blue arrows point to the furrows in the video still images.

Pressure on the friction ridge skin caused the shoulders (edges) of the surface ridge to push onto the surface of the glass as shown in Figure 15. The top diagram (A) of Figure 15 represents the contact edge of the ridge under medium deposition pressure. The bottom diagram (B) of Figure 15 represents the contact edge under high deposition pressure. Note that the depth of the furrow (ridge height) decreases under higher pressure.

Examination of friction ridge impressions left under varying degrees of pressure revealed subtle changes in the edge shapes of the ridges in the latent print. Note that the edges of the ridge (on the actual skin) are generally persistent until late age [19]. The changes in edge shapes described in this study refer to the latent print, not the skin. Under increasing pressure, the shoulders of the ridges pushed onto the surface and a different edge of the ridges made contact with the surface. The ridge edges in the latent prints appeared smoother as pressure increased. Additionally, as the deposition pressure increased, the depth of the furrows decreased, causing any incipient ridges or dots to contact the surface. The greater the pressure, the more prominent (larger) incipient ridges and dots became. Figure 16 shows latent prints from the same region of friction ridge skin under low, medium, and high deposition pressure (A, B, and C, respectively). Highlighted in these images are an indentation of a ridge (green) and an edge of a ridge (pink) that become increasingly smooth as pressure increases. Also highlighted are two incipient dots (blue arrows) that appear minimally under medium pressure and are prominent under high pressure.

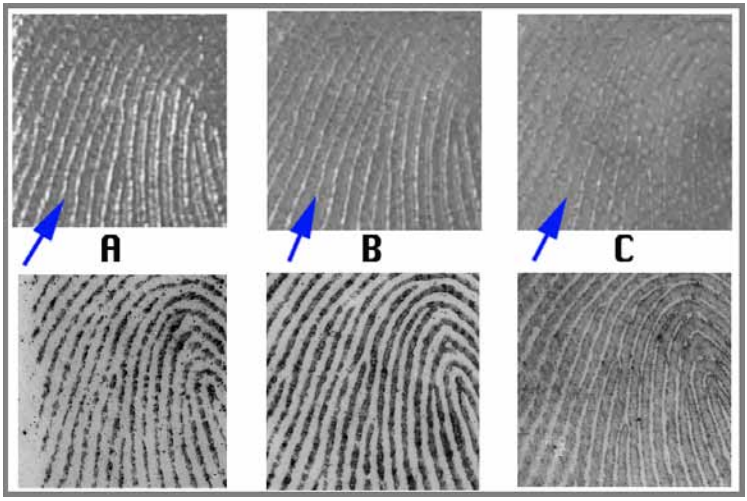

Figure 14

Ridge and furrow widths under low (A), medium (B), and high (C) deposition pressure. Arrows indicate the furrows in the video images.

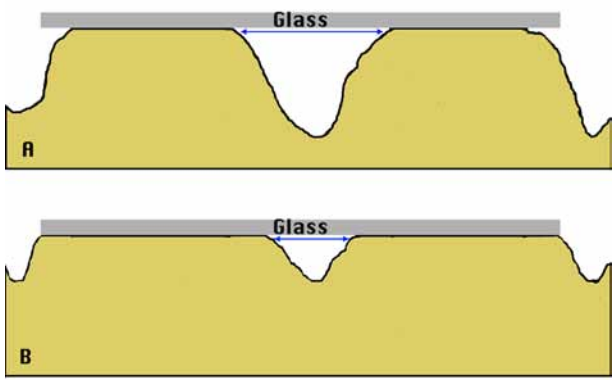

Figure 15

Contact region of the ridges under medium deposition pressure (A) and high deposition pressure (B). The blue arrows demonstrate the furrow widths.

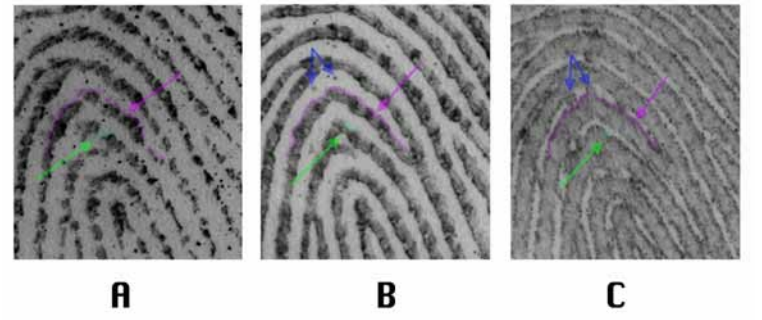

Figure 16

Latent prints created with low (A), medium (B), and high (C) deposition pressure. Diminishing edge shapes are shown in green and pink. Incipient dots (blue arrows) increasingly appear under medium (B) and high (C) pressure.

Sheering Stress

Sheering stress (distally, proximally, left, and right) was applied to the fingers to determine how the skin deforms when pushed in each direction. In this study, vertical or horizontal stress was applied to the fingers under low, medium, and high deposition pressure. As the deposition pressure increased, the amount of sheering stress required to move the stick region also increased. In other words, the firmer the finger was pressed into the glass, the longer the stick region held in place while the finger moved. Although the actual force of the vertical sheering stress was not measured, its general effects can be deduced from the distance the finger traveled before the stick area slipped ("gross slip") on the glass. The further the finger had to travel to move the stick area, the greater the sheering stress, and the more the skin deformed [2].

Vertical Sheering Stress

Vertical sheering stress, distally and proximally, was applied to the fingers. As expected, low pressure caused the least deformation for both the loop and the whorl. Under low pressure, gross slip occurred on the whorl after 0.6 mm to 1.1 mm proximally and 0.4 mm to 0.6 mm distally. Under low pressure, gross slip occurred on the loop after 0.1 mm to 0.2 mm proximally and 0.3 mm distally.

Under medium pressure, the direction of the vertical sheering stress affected the amount of deformation experienced by the skin; the skin experienced greater deformation when pushed distally. Approximately 1.9 mm was required to cause gross slip on the loop, and 1.6 mm to 2.0 mm was required to cause gross slip on the whorl when stress was applied distally. Proximally, however, gross slip occurred after approximately 0.5 mm on the loop and 1.3 mm to 1.6 mm on the whorl.

Distal sheering stress caused maximum deformation under high deposition pressure. Higher deposition pressure prevented the stick region from slipping until significant distal sheering stress was placed on the finger; approximately 2.9 mm was required to cause gross slip of the loop, and more than 3.0 mm was required to cause gross slip on the whorl. The anatomy of the finger pulp caused the skin to be more flexible in the distal direction. The tip of the bone pushed into the cushioned pulp of the tip of the finger, allowing the stick region to stay in place longer. Additionally, the flexible proximal finger pulp allowed the skin to compress against the stick region, rather than forcing the stick region to move. The longer the stick region was allowed to stay in place, the greater the deformation of the skin.

When proximal sheering stress was applied under high pressure, the whorl experienced gross slip at approximately 1.3 mm to 2.1 mm, and the loop experienced gross slip at approximately 0.6 mm to 0.7 mm. Raw data for distances needed to create gross slip for the loop and whorl under vertical sheering stress are summarized in Table 1.

	Distal Sheering Stress (mm)			**Proximal Sheering Stress (mm)**		
	Low	Medium	High	Low	Medium	High
Loop	0.3	1.9	2.9	0.1 to 0.2	0.5	0.6 to 0.7
Whorl	0.4 to 0.6	1.6 to 2	>3.0	0.6 to 1.1	1.3 to 1.6	1.3 to 2.1

Table 1

Raw data of distances needed to create gross slip under vertical sheering stress.

Table 1 must be considered with caution; there are only one or two trials per sheering stress. Some information, however, can be inferred from the data. The ranges between low, medium, and high pressure under distal sheering stress are distinct; there are significant gaps between the data. In the distal sheering stress videos, deformation increased dramatically as deposition pressure increased. The measurements from the distal sheering stress series are consistent with this observation. The ranges between low, medium, and high pressure under proximal sheering stress are too close to draw conclusions without further study.

Figures 17 and 18 are sequences of still images from the high deposition pressure/distal sheering stress videos. Figures 19 and 20 are sequences of still images from the high deposition pressure/proximal sheering stress videos. Each sequence has (A) the start position of the finger and selected minutiae, (B) the final position of the finger and selected minutiae prior to the stick region sliding on the glass, and (C) a composite image showing the distance the selected minutiae traveled. Note the significant distances traveled by minutiae in the proximal region of the finger pad when the sheering stress is applied distally (Figure 17C and Figure 18C).

In general, the further minutiae are located from the stick region, the greater the distance the minutiae are displaced. In Figures 17 and 18 (distal sheering stress), the minutiae between the core and the distal crease traveled further than any other minutiae tracked during the vertical sheering stress trials in this study.

There was notable compression and expansion of the furrows when vertical sheering stress was applied to the finger. When the finger was pushed distally ("up" in Figure 21), the furrows between the core and the tip of the finger expanded. The bone pushed into the fleshy tip of the finger, causing the ridges to stretch away from the immobile core (open accordion). The furrows between the core and the crease compressed as these ridges compacted against the immobile core (closed accordion). Once sufficient force was exerted on the finger, gross slip occurred. The ridges, however, remained spread apart on the tip and pressed together in the base until the stress was released.

When the fingers were pushed proximally ("down" in Figure 21), the opposite occurred: furrows between the tip and core compressed into the stick region, whereas the furrows between the core and crease expanded away from the stick region. Figure 21 demonstrates these effects.

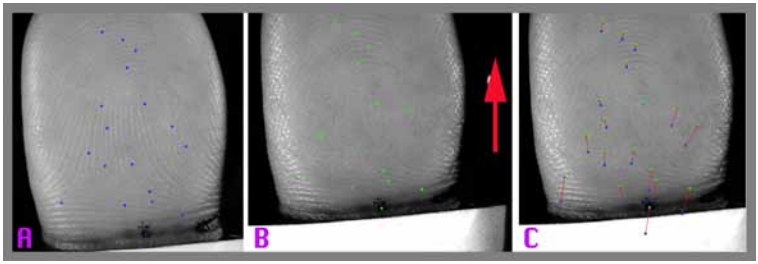

Figure 17

Distal sheering stress on loop under high deposition pressure. (A) Initial position of the finger and selected minutiae, (B) final position of the finger and selected minutiae, and (C) composite showing the linear displacement of the minutiae.

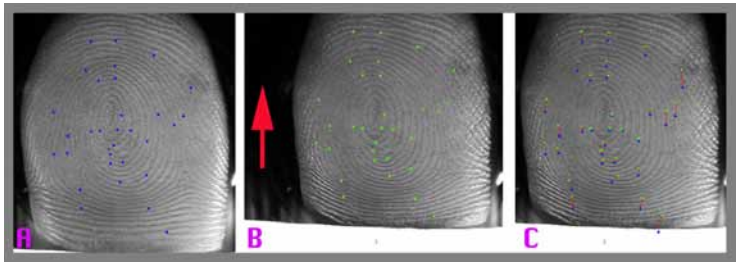

Figure 18

Distal sheering stress on whorl under high deposition pressure. (A) Initial position of the finger and selected minutiae, (B) final position of the finger and selected minutiae, and (C) composite showing the linear displacement of the minutiae.

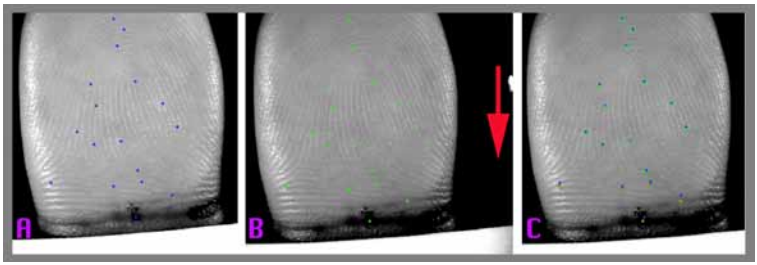

Figure 19

Proximal sheering stress on loop under high deposition pressure. (A) Initial position of the finger and selected minutiae, (B) final position of the finger and selected minutiae, and (C) composite showing the linear displacement of the minutiae.

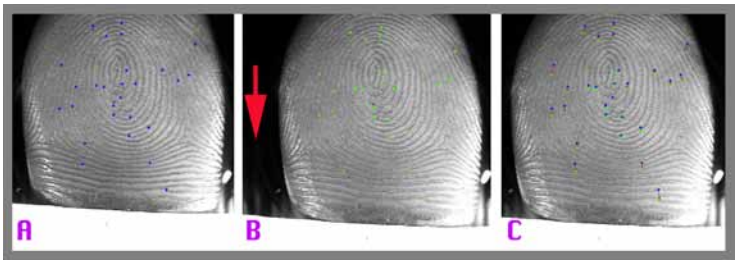

Figure 20

Proximal sheering stress on whorl under high deposition pressure. (A) Initial position of the finger and selected minutiae, (B) final position of the finger and selected minutiae, and (C) composite showing the linear displacement of the minutiae.

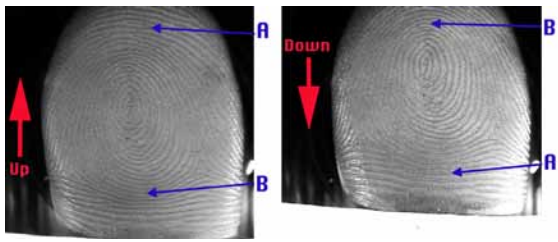

Figure 21

Expanded ridges (A) and compressed ridges (B) during distal ("Up") and proximal ("Down") sheering stress.

Latent prints created under vertical sheering stress contain visible clues that allow an analyst to determine the type of stress experienced by the skin. Figures 22 and 23 are latent prints created under high deposition pressure and distal sheering stress. Figures 24 and 25 are latent prints created under high deposition pressure and proximal sheering stress.

The latent print in Figure 22 was created by pushing the loop index finger distally 4 mm under high deposition pressure. The latent print in Figure 22 can be dissected as follows: A - Initial contact position of the base of the finger (where the finger first touched the glass); B - Drag smear created by the ridges above the distal crease sliding through residue deposited on the initial touch of the finger (the ridges in this region compressed and smeared the residue on the glass); C - Vertical drag lines indicating vertical direction of movement; D - The outflow of the core was pushed horizontally (compared to the standard) as the ridges compressed against the stick region; E - Creases appeared because of the extreme stress on the skin causing the skin to buckle (wrinkle) as the ridges pushed against the stick region; F - Expanded furrows at the tip of the finger; G - Edges of the print can have misaligned or incorrectly stitched ridges (ridges that appear continuous, but are parts of different ridges that have aligned) and must be analyzed with caution.

The latent print in Figure 23 was created by pushing the whorl index finger distally 4 mm under high deposition pressure. The latent print in Figure 23 can be dissected as follows: A - Initial contact position of the base of the finger (where the finger first touched the glass); B - Drag smear created by the ridges above the distal crease sliding through residue deposited on the initial touch of the finger (the ridges in this region compressed and smeared the residue on the glass); C - Vertical drag lines indicating vertical direction of movement; D - Compressed furrows as the ridges pushed against the stick region; E - Band of thick ridges because of the extreme stress on the skin causing slight longitudinal (along the ridge rather than across ridges) compression of the ridges; F - Expanded furrows at the tip of the finger; G - Edges of the print can have misaligned or incorrectly stitched ridges (ridges that appear continuous, but are parts of different ridges that have aligned) and must be analyzed with caution.

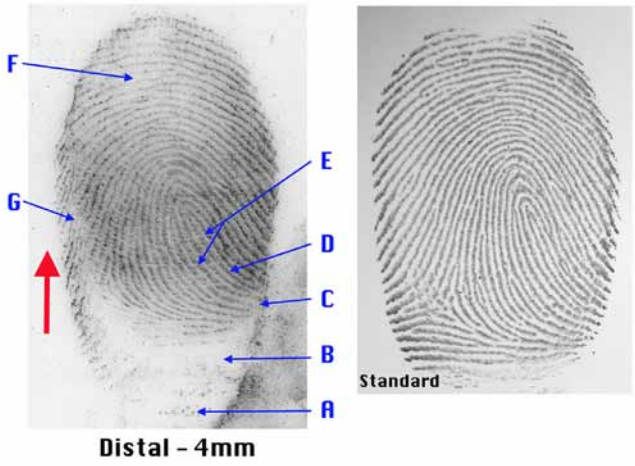

Figure 22

Distal sheering stress 4 mm on loop pattern under high deposition pressure.

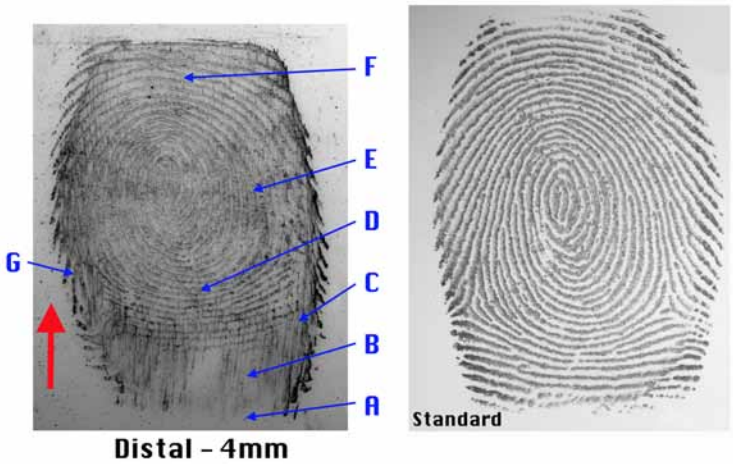

Figure 23

Distal sheering stress 4 mm on a whorl pattern under high deposition pressure.

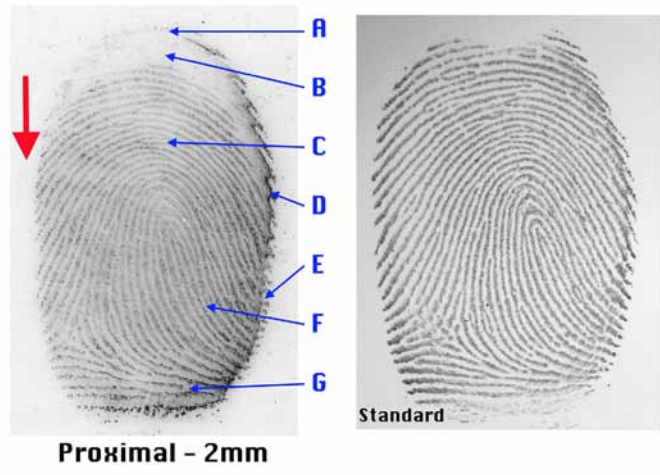

Figure 24

Proximal sheering stress 2 mm on loop pattern under high deposition pressure.

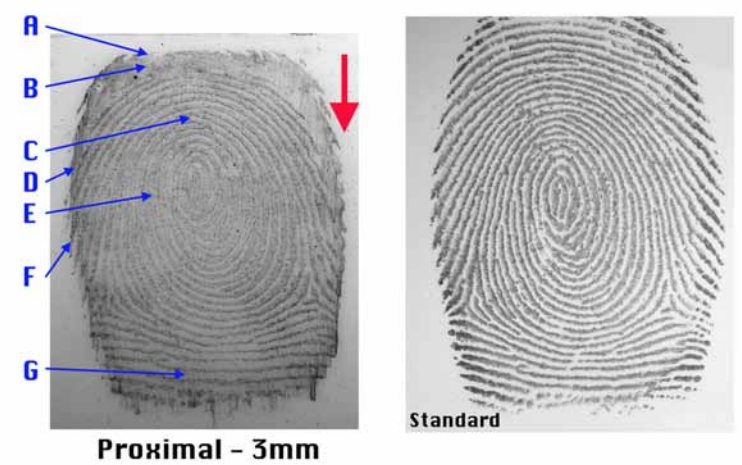

Figure 25

Proximal sheering stress 3 mm on whorl under high deposition pressure.

The latent print in Figure 24 was created by pulling the loop index finger proximally 2 mm under high deposition pressure. The latent print in Figure 24 can be dissected as follows: A - Initial contact position of the tip of the finger (where the finger first touched the glass); B - Drag smear created by the ridges on the tip sliding through residue deposited on the initial touch of the finger (the ridges in this region were under light pressure because of the convex shape of the tip of the finger and smeared the residue on the glass); C - Compressed furrows above the core as the ridges pushed against the stick region; D - Vertical drag lines indicating vertical direction of movement; E - Edges of the print can have misaligned or incorrectly stitched ridges (ridges that appear continuous, but are parts of different ridges that have aligned) and must be analyzed with caution; F - The outflow of the core is pulled vertically (compared to the standard) as the ridges stretched down from the stick region; G - Expanded furrows at the base of the finger.

The latent print in Figure 25 was created by pulling the whorl index finger in the proximal direction 3 mm under high deposition pressure. The latent print in Figure 25 can be dissected as follows: A - Initial contact position of the tip of the finger (where the finger first touched the glass); B - Drag smear created by the ridges on the tip sliding through residue deposited on the initial touch of the finger (the ridges in this region were under light pressure because of the convex shape of the tip of the finger and smeared the residue on the glass); C - Compressed furrows above the core as the ridges pushed against the stick region; D - Vertical drag lines indicating vertical direction of movement; E - Band of thick ridges because of the extreme stress on the skin causing slight longitudinal (along the ridge rather than across ridges) compression of the ridges; F - Edges of the print can have misaligned or incorrectly stitched ridges (ridges that appear continuous, but are parts of different ridges that have aligned) and must be analyzed with caution; G - Expanded furrows at the base of the finger.

Horizontal Sheering Stress

Horizontal sheering stress was explored to determine the manner in which the skin deforms when the finger is pushed to the left or right. In this study, the fingers were moved left and right under low, medium, and high deposition pressure.

As expected, the least deformation for both the loop and the whorl took place under low pressure. Under low pressure, gross slip occurred after the whorl moved 0.4 mm to 0.5 mm left and 0.4 mm to 0.6 mm right. Under low pressure, gross slip occurred after the loop moved 0.6 mm to 0.8 mm left and 0.3 mm to 0.4 mm right.

Under medium pressure, the loop experienced gross slip at approximately 1 mm left and right. Under high pressure, the loop experienced gross slip at approximately 1 mm left and 1.2 mm to 1.3 mm right. Under medium pressure, the whorl experienced gross slip at approximately 0.7 mm left and 0.4 mm to 0.7 mm right. Under high pressure, the whorl experienced gross slip at approximately 0.6 mm to 0.7 mm left and 0.3 to 0.6 mm right. Raw data for distances needed to create gross slip for the loop and whorl under horizontal sheering stress are summarized in Table 2.

	Left Sheering Stress (mm)			**Right Sheering Stress (mm)**		
	Low	Medium	High	Low	Medium	High
Loop	0.6 to 0.8	1.0	1.0	0.3 to 0.4	1.0	1.2 to 1.3
Whorl	0.4 to 0.5	0.7	0.6 to 0.7	0.4 to 0.6	0.4 to 0.7	0.3 to 0.6

Table 2

Summary of distances needed to create gross slip under horizontal sheering stress.

Again, the data in Table 2 must be considered with caution. The data under low, medium, and high pressure (both left and right) for both fingers is too close to draw many conclusions. The loop, however, may be more flexible (i.e., experienced more deformation) than the whorl, both left and right, under medium and high pressure; the loop appeared more flexible in the videos (see Figures 26 through 29).

Figures 26, 27, 28, and 29 are sequences of still images from the high deposition pressure/horizontal sheering stress videos. Each sequence has (A) the start position of the finger and selected minutiae, (B) the final position of the finger and selected minutiae prior to the stick region sliding on the glass, and (C) a composite image showing the distance the selected minutiae traveled.

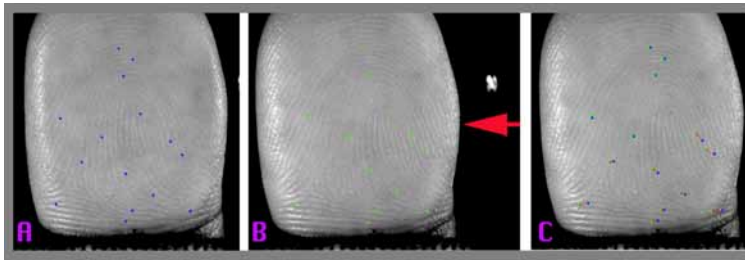

Figure 26

Horizontal sheering stress left on loop under high deposition pressure. (A) Initial position of the finger and selected minutiae, (B) final position of the finger and selected minutiae, and (C) composite showing the linear displacement of the minutiae.

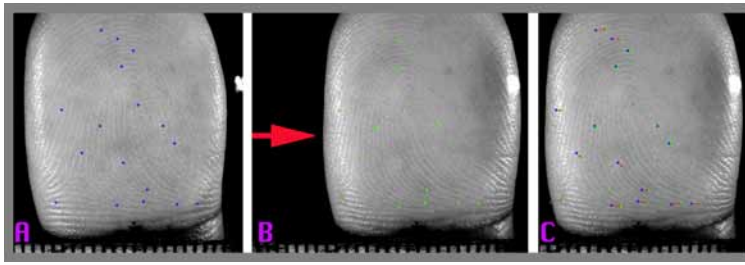

Figure 27

Horizontal sheering stress right on loop under high deposition pressure. (A) Initial position of the finger and selected minutiae, (B) final position of the finger and selected minutiae, and (C) composite showing the linear displacement of the minutiae.

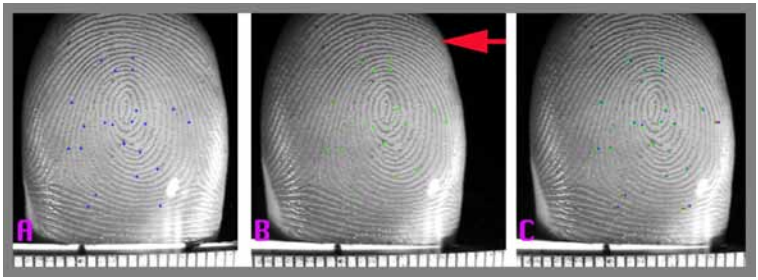

Figure 28

Horizontal sheering stress left on whorl under high deposition pressure. (A) Initial position of the finger and selected minutiae, (B) final position of the finger and selected minutiae, and (C) composite showing the linear displacement of the minutiae.

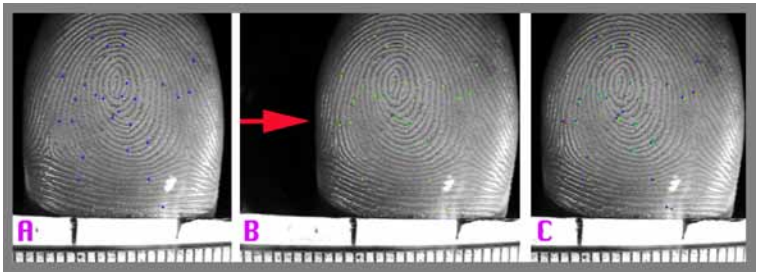

Figure 29

Horizontal sheering stress right on whorl under high deposition pressure. (A) Initial position of the finger and selected minutia, (B) final position of the finger and selected minutia, and (C) composite showing the linear displacement of the minutia.

There was notable compression and expansion of the furrows when horizontal sheering stress was applied to the finger. Once again, the location of the ridges on either side of the stick region determined whether the furrows expanded or compressed. The furrows on the edge of the finger leading the movement expanded as the bone pulled the edge of the finger away from the stick region. (The furrows on the left side of the finger expanded when the finger was pushed to the left.) The furrows on the trailing edge of the finger compressed against the stick region as the finger moved horizontally. (The furrows on the right side of the finger compressed when the finger was pushed left.) Figure 30 demonstrates these effects.

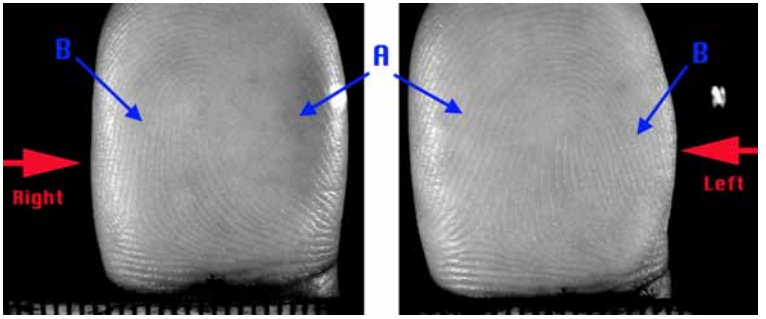

Figure 30

Expanded ridges (A) on the edge of the finger leading the movement of the finger (right edge of finger moving right and left edge of finger moving left). Compressed ridges (B) on the trailing edge of the finger.

Latent prints created under horizontal sheering stress contain visible clues that allow an analyst to determine the type of stress experienced by the skin. Figures 31 and 32 are latent prints created with the loop pattern under high deposition pressure and horizontal sheering stress left and right. Figures 33 and 34 are latent prints created with the whorl pattern under high deposition pressure and horizontal sheering stress left and right.

The latent print in Figure 31 was created by pushing the loop index finger left 3 mm under high deposition pressure. The latent print in Figure 31 can be dissected as follows: A - Initial contact position of the finger (finger rolled off the surface as it was pushed to the left, leaving a line of clean ridges along the right edge); B - Drag smear created by the compressed ridges smearing through residue placed on the surface during the initial contact with the glass (the drag smear has horizontal drag lines); C - Compressed ridges on the trailing edge of the print (ridges compressed against core stick region); D - Ridge flow of core is angled vertically compared to the standard because of ridges compressed against core; E - Edges of the print can have misaligned or incorrectly stitched ridges (ridges that appear continuous, but are parts of different ridges that have aligned) and must be analyzed with caution; F - Expanded ridges on the leading edge of the print (ridges pulled away from the core stick region).

The latent print in Figure 32 was created by pushing the loop index finger right 3 mm under high deposition pressure. The latent print in Figure 32 can be dissected as follows: A - Initial contact position of the finger (finger rolled off the surface as it was pushed to the right, leaving a line of clean ridges along the left edge); B - Drag smear created by the compressed ridges smearing through residue placed on the surface during the initial contact with the glass (drag smear has horizontal drag lines); C - Compressed ridges on the trailing edge of the print (ridges compressing against core stick region); D - Duplication of ridges can occur in the drag smear and must be analyzed carefully; E - Expanded ridges on the leading edge of the print (ridges pulled away from the core stick region); F - Ridge flow out of core is angled horizontally compared to the standard because of the pulling of the ridges to the right; G - Edges of the print can have misaligned or incorrectly stitched ridges (ridges that appear continuous, but are parts of different ridges that have aligned) and must be analyzed with caution.

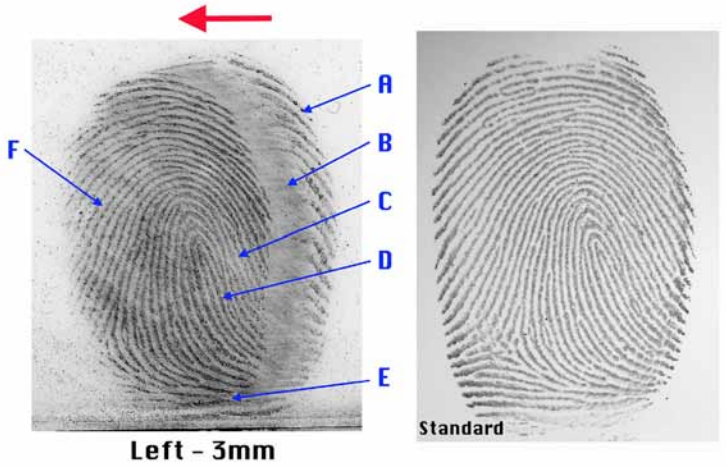

Figure 31

Horizontal sheering stress 3 mm left on loop under high deposition pressure.

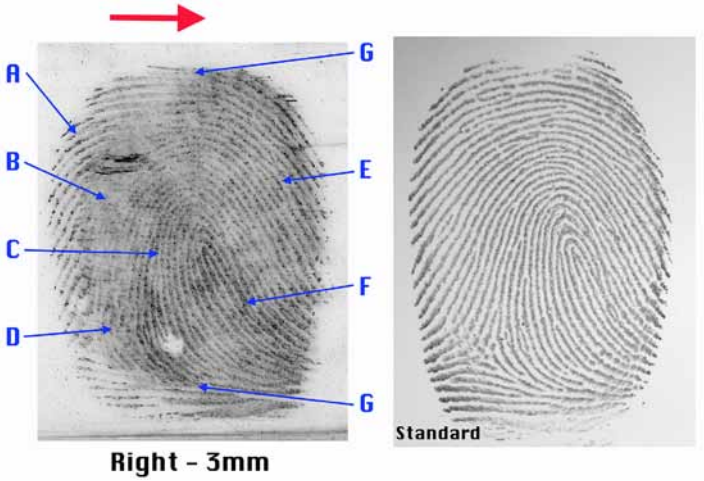

Figure 32

Horizontal sheering stress 3 mm right on loop under high deposition pressure.

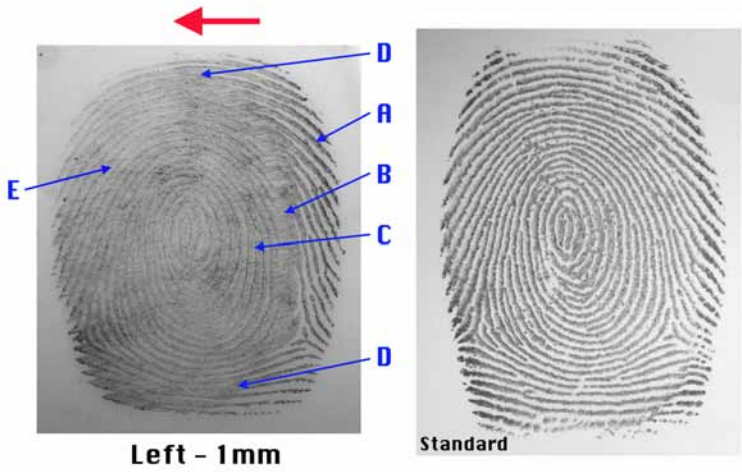

Figure 33

Horizontal sheering stress 1 mm left on whorl under high deposition pressure.

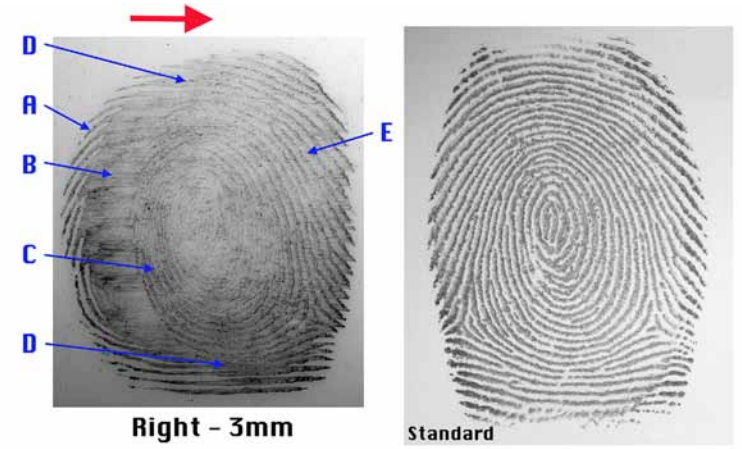

Figure 34

Horizontal sheering stress 3 mm right on whorl under high deposition pressure.

The latent print in Figure 33 was created by pushing the whorl index finger left 1 mm under high deposition pressure. The latent print in Figure 33 can be dissected as follows: A - Initial contact position of the finger (finger rolled off the surface as it was pushed to the left, leaving a line of clean ridges along the right edge); B - Drag smear created by the compressed ridges smearing through residue placed on the surface during the initial contact with the glass (drag smear has horizontal drag lines); C - Compressed ridges on the trailing edge of the print (ridges compressing against core stick region); D - Edges of the print can have misaligned or incorrectly stitched ridges (ridges that appear continuous, but are parts of different ridges that have aligned) and must be analyzed with caution; E - Expanded ridges on the leading edge of the print (ridges pulled away from the core stick region).

The latent print in Figure 34 was created by pushing the whorl index finger right 3 mm under high deposition pressure. The latent print in Figure 34 can be dissected as follows: A - Initial contact position of the finger (finger rolled off the surface as it was pushed to the right, leaving a line of clean ridges along the left edge); B - Drag smear created by the compressed ridges smearing through residue placed on the surface during the initial contact with the glass (drag smear has horizontal drag lines); C - Compressed ridges on the trailing edge of the print (ridges compressing against core stick region); D - Edges of the print can have misaligned or incorrectly stitched ridges (ridges that appear continuous, but are parts of different ridges that have aligned) and must be analyzed with caution; E - Expanded ridges on the leading edge of the print (ridges pulled away from the core stick region).

Torque

Torque was applied to the fingers to determine the effects of twisting on the friction ridge skin. The loop and whorl were rotated clockwise and counter-clockwise under low, medium, and high deposition pressure. Early video indicated that the whorl experienced similar, although mirrored, deformation, regardless of the direction of the torque. As a result, only counter-clockwise rotation was recorded and measured. As expected, little deformation occurred under low deposition pressure; gross slip for the loop and whorl occurred after less than 9° in either direction.

Increasing deposition pressure increased the amount of deformation experienced by the loop and the whorl. Under medium deposition pressure, the whorl experienced gross slip at approximately 7.1° to 9.8° rotation.

Deformation of the loop pattern, however, depended on the direction of rotation. The right slant loop was more flexible rotating counter-clockwise (with the ridge flow) than clockwise (against the delta). The asymmetry of the loop ridge flow is likely the reason for the difference in flexibility. When rotating counter-clockwise, the rotation mirrored the curvature of the outflow of the core, and the series of parallel ridges in this region absorbed the deformation by curving with the force. Under medium pressure, gross slip occurred after approximately 11.8° to 17.5° rotation counter-clockwise. In the opposite direction, however, the ridges in the core region were straightened as they pushed against the vertical ridges flowing up from the delta region. The ridges were not very flexible as they straightened and forced gross slip to occur approximately 8.6° to 10.6° clockwise twist under medium pressure.

Under high compressive stress, the whorl experienced gross slip at approximately 27.6° to 30° rotation. Once again, the effects of counter-clockwise rotation simply mirrored the effects of clockwise rotation in the whorl pattern. Under high deposition pressure, the loop also experienced significantly greater deformation counter-clockwise because of the outflow of ridges from the core. Gross slip occurred after approximately 18.2° to 26.7° counter-clockwise (with the ridge flow) rotation and after approximately 8.9° to 12.8° rotation clockwise (against the delta) rotation. Raw data for degree of twist needed to create gross slip for the loop and whorl under torque are summarized in Table 3.

	Counter-clockwise			Clockwise		
	Low	Medium	High	Low	Medium	High
Loop	4.3° to 6.1°	11.8° to 17.5°	18.2° to 26.7°	< 1°	8.6° to 10.6°	8.9° to 12.8°
Whorl	6° to 8.6°	7.1° to 9.8°	27.6° to 30°	-	-	-

Table 3

Summary of degree of twist needed to create gross slip under torque.

The distance traveled by minutiae was highest on the periphery of the print and decreased as the minutiae were positioned closer to the core stick region. This would be expected as simple physics dictates that the angular velocity would be higher on the periphery of the print. Another way to consider this phenomenon with the whorl is to think of a series of concentric rings where the outer rings rotate first and are joined, one by one, by the inner rings until all the rings are rotating together.

Figures 35, 36, and 37 are sequences of still images from the high compressive stress and torque videos. Each sequence has (A) the start position of the finger and selected minutiae, (B) the final position of the finger and selected minutiae prior to the stick region rotating on the glass, and (C) a composite image showing the distance the selected minutiae traveled.

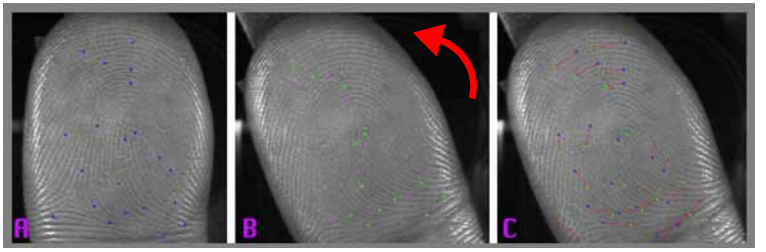

Figure 35

Counter-clockwise torque on loop under high deposition pressure. (A) Initial position of the finger and selected minutiae, (B) final position of the finger and selected minutiae, and (C) composite showing the linear displacement of the minutiae.

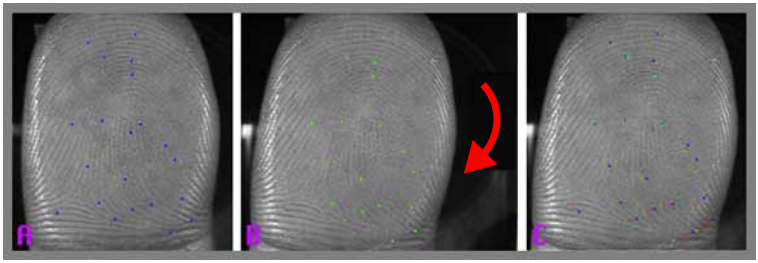

Figure 36

Clockwise torque on loop under high deposition pressure. (A) Initial position of the finger and selected minutiae, (B) final position of the finger and selected minutiae, and (C) composite showing the linear displacement of the minutiae.

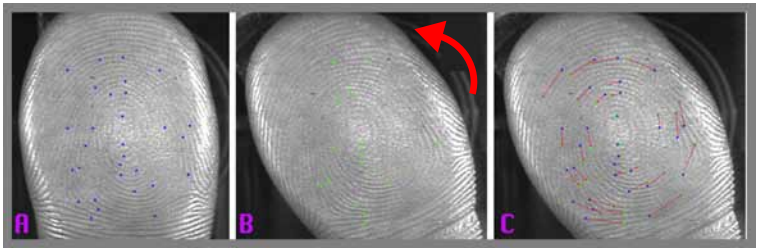

Figure 37

Counter-clockwise torque on whorl under high deposition pressure. (A) Initial position of the finger and selected minutiae, (B) final position of the finger and selected minutiae, and (C) composite showing the linear displacement of the minutiae.

Latent prints created under torque contain visible clues that allow an analyst to determine the type of stress experienced by the skin. Figures 38 and 39 are latent prints created with the loop pattern under high deposition pressure and torque counter-clockwise and clockwise. Figure 40 is a latent print created with the whorl pattern under high deposition pressure and counter-clockwise torque.

The latent print in Figure 38 was created by rotating the loop index finger 45° counter-clockwise under high deposition pressure. The latent print in Figure 38 can be dissected as follows: A - Initial contact position of the finger (where the finger first touched the glass); B - Curved drag lines indicating twisting motion; C - Core stick region with clear ridges and furrows (this region experienced very little movement); D - Ridge flow of core is more curved (compared to standard) because of the ridges curving with the rotation of the finger; E - Residue build-up on leading edge of the ridges (these ridges are pushed through residue and the leading edge of the ridge acts as a "squeegee", accumulating residue and causing background noise in the furrows).

The latent print in Figure 39 was created by rotating the loop index finger 45° clockwise under high deposition pressure. The latent print in Figure 39 can be dissected as follows: A - Initial contact position of the finger (where the finger first touched the glass); B - Curved drag lines indicating twisting motion; C - Core stick region with clear ridges and furrows (this region experienced very little movement); D - Core develops an abnormal ridge flow because of ridges between the core and the delta bending with the rotation of the finger; E - Residue build-up on leading edge of the ridges (these ridges are pushed through residue and the leading edge of the ridge acts as a "squeegee", accumulating residue and causing background noise in the furrows).

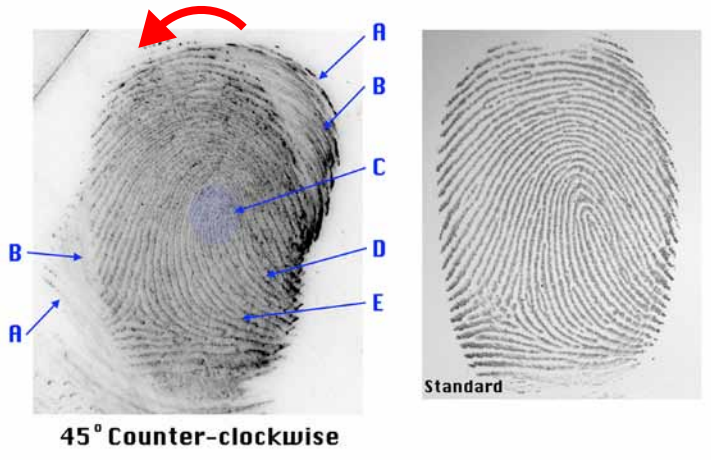

Figure 38

45° counter-clockwise rotation of loop under high deposition pressure.

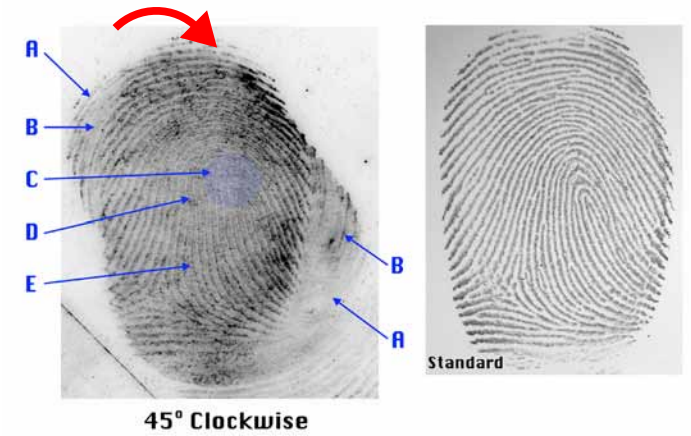

Figure 39

45° clockwise rotation of loop under high deposition pressure.

The latent print in Figure 40 was created by rotating the whorl index finger 45° counter-clockwise under high deposition pressure. The latent print in Figure 40 can be dissected as follows: A - Initial contact position of the finger (where the finger first touched the glass); B - Curved drag lines indicating twisting motion; C - Core stick region with clear ridges and furrows (this region experienced very little movement) and note the angle of the core to the delta in the latent print compared to the standard; D - Circular ridges rotating through residue causes background noise (smearing) in the furrows and the edges of the ridges to contain more residue than the surface of the ridge (as a result, the edges of the ridge develop with powder and the ridges in this region appear outlined with the black powder); E - As the skin moves onto a clean region of the glass, the residue becomes thinner and the ridges are no longer evenly coated with residue (as a result, the ridges appear patchy when developed with black powder).

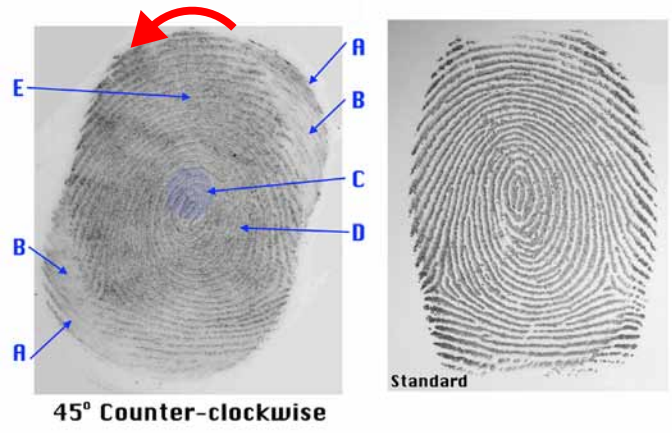

Figure 40

45° counter-clockwise rotation of whorl under high deposition pressure.

Conclusions

Systematic study of simple skin deformation on a smooth, rigid surface revealed trends in both the skin's response to stress and the appearance of latent prints generated with the different stresses. As deposition pressure increased, the surface area of contact between the finger and the glass also increased (creating a larger latent print). Additionally, as deposition pressure increased, the ridges became wider and the furrows more narrow. The wider ridges created by increased pressure presented smoother edge shapes in the latent prints. Increased pressure also caused incipient ridges to become more prominent. When sheering stresses were applied to the fingers, the skin deformed significantly more in the distal direction than proximal, left, or right. The latent prints generated by the different sheering stresses presented robust clues that indicated direction of stress (e.g., compression and expansion of ridges on the trailing edge and leading edge, respectively). Torque also created significant deformation, affecting the position of minutiae on the periphery of the finger relative to the core. Deformation that was due to torque was influenced by the symmetry of the fingerprint pattern; the loop demonstrated greater flexibility when torque followed the outflow of the core versus against the delta. The direction of tangential stress, local ridge flows, and the underlying structures of the fingers and skin provide limits to skin deformation and aid in the explanation of distortion in latent prints.

Skin deformation, however, is just one piece of the distortion puzzle that must be considered when examining latent prints collected during casework. Latent prints collected from crime scenes or items of evidence may exhibit a myriad of distortion issues. The latent prints may contain reproductions of permanent or temporary biological distortions of the skin. Biological distortions include scars, warts, superficial damage, and so forth. The type and location of residue on the friction ridge skin creates distortion issues: partial tonal reversals, patchy ridges, outlined edges of ridges, and so forth. The manner in which the skin contacts the surface creates distortion (skin deformation). The surface itself can cause distortion. Surface distortions can be created by rigid or flexible surfaces, flat or curved surfaces, textured or smooth surfaces, clean or dirty surfaces, and wet or dry surfaces. Distortion can occur postdeposition because of environmental causes (e.g., heat or rain) or physical disruption

(abrasion). The development technique may also cause distortion issues (e.g., spotted ninhydrin prints or powder masking edge shapes).

A thorough study and analysis of all types of distortion will provide practitioners with a database of knowledge from which to draw reasonable inferences. Practitioners must acknowledge there are unknown factors that could come into play during the deposition of a latent print. As a result, some distortions may be subject to interpretation or may be unintelligible.

Despite the potential complexity of latent prints recovered during casework, there are prints collected from smooth rigid surfaces that exhibit evidence of simple skin deformations. Figure 41 is a latent print recovered from the exterior of a vehicle. This print, particularly the abnormal ridge flow of the core, shows strong evidence of counter-clockwise twist: A - Initial contact of the tip of the finger; B - Curved drag lines; C - Misaligned ridges; D - Core appears unusually vertical and there is an abnormal arch in the core ridge flow; E - Smearing at the tip of the finger likely caused by residue concerns; and F - Deflated tape bubbles.

Figure 42 is a latent print recovered from the right side of a knife blade. In this print, there is significant evidence of sheering stress up and to the right (northeast if referencing the distal end of the finger as north): A - Initial contact of the finger to the blade; B - Drag smear; C - Compressed ridges pushing against the core stick region; D - Diagonal drag lines in the drag smear; E - Misaligned ridges; F - Tip of the finger rolling onto the blade; and G - Separated ridges on the leading edge of the finger.

Although not a panacea of distortion explanations, simple skin deformation certainly accounts for some distortions encountered during the analysis of latent prints. The robust, visible clues found in latent prints can be explained through knowledge of the structural components of the hand that contribute to skin flexibility. Why are these ridges compressed together? Because they are pushing into the region of stick created by the distal tuft of the bone. Why are minutiae on the periphery of the print so out of alignment with the core? Because the finger twisted on the surface and the angular velocity at the edge of the print is higher, causing minutiae further from the core to travel greater distances.

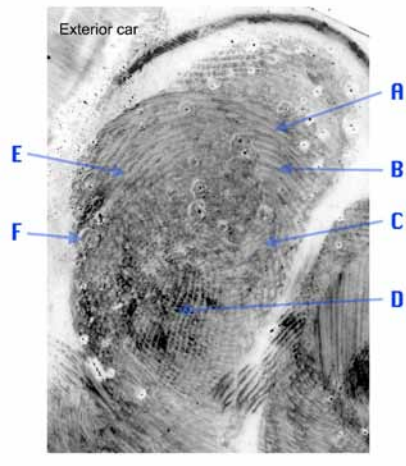

Figure 41

Latent print recovered from the exterior of a car.

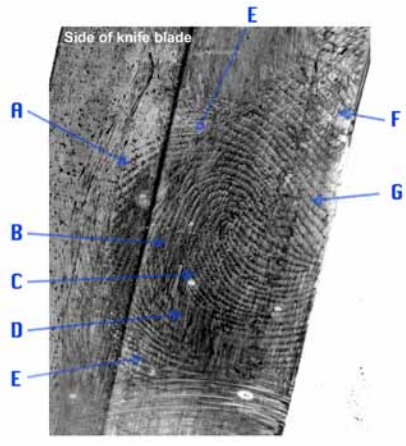

Figure 42

Latent print recovered from right side of a knife blade.

Additional research is needed to address deformation of all areas of the hand (palm regions and phalanges) under different parameters. Parameters that require research include surfaces (e.g., porous surfaces and curved surfaces), types of residue (e.g., eccrine sweat or blood), angle of touch, changes in pressure, combined stresses, and so forth. The results of this study are limited to the factors set forth (index fingers charged with sebaceous secretions on a clean glass surface) and should not be construed beyond those factors.

"Distortion" is not a wild card to be played to dismiss unexplainable regions of concern in a latent print. Concentrated study of basic skin deformation and all aspects of distortion will provide knowledge-based tools for the proper assessment of friction ridge impressions.

Acknowledgments

This research would not have been possible without the endless patience of my finger donor, Isaac Maceo. The two years of filming hundreds of video clips has earned him my undying gratitude and a fingerprint medal of honor. I would like to thank the latent print section and lab director of the Las Vegas Metropolitan Police Department Forensic Lab for their constant moral and intellectual support over the last four years as this research evolved. Additionally, I would like to thank numerous colleagues and students for entertaining endless discussions on skin deformation and helping me formulate a method for publishing on paper what is best demonstrated by skin flicks.

For further information, please contact:

Alice Maceo
Las Vegas Metropolitan Police Department - Forensic Laboratory
5605 West Badura Avenue, Suite 120 B
Las Vegas, NV 89118-4705
alicemaceo@earthlink.net

References

1. Cappelli, R.; Maio, D.; Maltoni, D. Modelling Plastic Distortion in Fingerprint Images. In *Proceedings of the Second International Conference on Advances in Pattern Recognition*; Singh, S., Murshed, N. A., Kropatsch, W. G., Eds.; Springer-Verlag: London, 2001; pp 369-376.
2. Ikeda, A.; Kurita, Y.; Ueda, J.; Matsumoto, Y.; Ogasawara, T. Grip Force Control for an Elastic Finger Using Vision-Based Incipient Slip Feed-Back. In *Proceedings of IEEE/RSJ International Conference on Intelligent Robots and Systems*; IEEE: Piscataway, NJ, 2004; pp 810-815.
3. Ross, A.; Dass, S.; Jain, A. Fingerprint Warping Using Ridge Curve Correspondences. *IEEE Transactions on Pattern Analysis and Machine Intelligence*; **2006**, *28* (1), 19-30.
4. Dorai, C.; Ratha, N. K.; Bolle, R. M. Dynamic Behavior Analysis in Compressed Fingerprint Videos. *IEEE Transactions on Circuits and Systems for Video Technology* **2004**, *14* (1), 58-73.
5. Kurita, Y.; Ikeda, A.; Ueda, J.; Ogasawara, T. A Fingerprint Pointing Device Utilizing the Deformation of the Fingerprint During Incipient Slip. *IEEE Transactions on Robotics* **2005**, *21* (5), 801-811.
6. Hearn, E. J. *Mechanics of Material: An Introduction to the Mechanics of Elastic and Plastic Deformation of Solids and Structural Materials*, 3rd ed.; Butterworth-Heinemann: Boston, 1997; p 3.
7. Johnson, K. L. *Contact Mechanics*; Cambridge University Press: United Kingdom, 1987; pp 84-106.
8. Cowger, J. F. *Friction Ridge Skin: Comparison and Identification of Fingerprints*; CRC Press: New York, 1993; pp 186-188.
9. Ashbaugh, D. R. *Quantitative-Qualitative Friction Ridge Analysis: An Introduction to Basic and Advanced Ridgeology*; CRC Press: New York, 1999; pp 123-128.
10. Maltoni, D.; Maio, D.; Jain, A. K.; Prabhakar, S. *Handbook of Fingerprint Recognition*; Springer-Verlag: New York, 2003; pp 160-164.
11. Senior, A.; Bolle, R. Improved Fingerprint Matching by Distortion Removal. *IEICE Trans. Information and Systems* **2001**, *84* (7), 825-831.
12. Serina, E. R.; Mockensturm, E.; Mote, C. D. Jr.; Rempe, D. A Structural Model of the Forced Compression of the Fingertip Pulp. *J. Biomech*. **1998**, *31* (7), 639-646.

13. Neumann, C.; Champod, C.; Puch-Solis, R.; Egli, N.; Anthonioz, A.; Bromage-Griffiths, A. Computation of Likelihood Ratios in Fingerprint Identification for Configurations of Any Number of Minutiae. *J. For. Sci.* **2007**, *52* (1), 54-64.
14. Schmidt, H.; Lanz, U. *Surgical Anatomy of the Hand*; Thieme: New York, 2004.
15. Cummins H.; Midlo, C. *Finger Prints, Palms, and Soles: An Introduction to Dermatoglyphics*; Blakiston: Philadelphia, 1943; p 54.
16. Lavker, R.; Sun, T. Epidermal Stem Cells. *J. Invest. Dermatol.* **1983**, *81* (1 Supp.), 121s-127s.
17. Swensson, O.; Langbein, L.; McMillan, J. R.; Stevens, H. P.; Leigh, I. M.; McLean, W. H.; Lane, E. B.; Eady, R. A. Specialized Keratin Expression Pattern in Human Ridges Skin as an Adaptation to High Physical Stress. *Br. J. Dermatol.* **1998**, *139* (5), 767-775.
18. Pawluk, D.; Howe, R. D. Dynamic Contact of the Human Fingerpad Against a Flat Surface. *J. Biomech. Eng.* **1999**, *121* (6), 605-611.
19. Okajima, M. Dermal and Epidermal Structures of the Volar Skin. Birth Defects: Orig. Artic. Ser. 1979, 15 (6), 179-198.